EURASIP Journal on Advances in Signal Processing
a SpringerOpen Journal

RESEARCH Open Access

# Sparse reconstruction for direction-of-arrival estimation using multi-frequency co-prime arrays

Elie BouDaher, Fauzia Ahmad* and Moeness G Amin

**Abstract**

In this paper, multi-frequency co-prime arrays are employed to perform direction-of-arrival (DOA) estimation with enhanced degrees of freedom (DOFs). Operation at multiple frequencies creates additional virtual elements in the difference co-array of the co-prime array corresponding to the reference frequency. Sparse reconstruction is then used to fully exploit the enhanced DOFs offered by the multi-frequency co-array, thereby increasing the number of resolvable sources. For the case where the sources have proportional spectra, the received signal vectors at the different frequencies are combined to form an equivalent single measurement vector model corresponding to the multi-frequency co-array. When the sources have nonproportional spectra, a group sparsity-based reconstruction approach is used to determine the direction of signal arrivals. Performance evaluation of the proposed multi-frequency approach is performed using numerical simulations for both cases of proportional and nonproportional source spectra.

**Keywords:** Sparse reconstruction; Co-prime arrays; DOA estimation; Group sparsity

## 1 Introduction

Direction-of-arrival (DOA) estimation has been an area of continued research interest due to its wide range of applications in radar, sonar, and wireless communications [1-3]. A main parameter in DOA estimation is the maximum number of sources that can be resolved. Traditional high-resolution DOA techniques, such as MUSIC [4] and ESPRIT [5], can only estimate up to $(N-1)$ sources when applied to an $N$ element uniform linear array (ULA). Numerous nonuniform array geometries and signal processing techniques have been introduced to increase the number of resolvable sources beyond that offered by a ULA for a given number of physical sensors [6-13].

Minimum redundancy arrays (MRAs) and minimum hole arrays (MHAs) are two common classes of nonuniform linear arrays [6-9]. Both MRAs and MHAs provide the ability to resolve more sources than the number of physical sensors by reducing the number of redundant virtual elements in the difference co-array. The difference co-array is defined as the set of all pairwise differences of array element locations, and thus, it specifies the set of 'lags' at which the spatial correlation function may be estimated [10,11]. For a given number of physical sensors, MRAs are arrays with the lowest possible redundancy and without any missing lags or 'holes' in the corresponding co-array, whereas MHAs (also known as Golomb arrays) have a minimum number of holes and zero redundancy. More recently, nested co-prime array configurations have been proposed [12,13]. Nested structure is obtained by systematically nesting two uniform linear subarrays, with one subarray assuming a unit inter-element spacing, and can provide $O(N^2)$ degrees of freedom (DOFs)_ using only $N$ physical sensors. A nested array generates a co-array with no holes. The co-prime array consists of two uniform linear subarrays having $M$ and $N$ sensors with specific inter-element spacings, where $M$ and $N$ are co-prime, and offers $O(MN)$ degrees of freedom. The co-prime array produces a co-array that has both redundancy and holes.

High-resolution DOA estimation with nonuniform arrays can be accomplished based on two main approaches, namely, covariance matrix augmentation [14] and spatial smoothing method for covariance matrix construction [12,13,15]. In the former approach, the constructed augmented covariance matrix is not guaranteed to be positive semi-definite and requires positive definite Toeplitz completion [16,17]. The latter approach vectorizes the covariance matrix of the nonuniform array to emulate

* Correspondence: fauzia.ahmad@villanova.edu
Center for Advanced Communications, Villanova University, Villanova, PA 19085, USA

observations at a virtual array whose sensor positions are given by the difference co-array. Since the source signals are replaced by their powers in this case, rendering the source environment coherent, spatial smoothing is utilized to decorrelate the sources and to restore the rank of the corresponding covariance matrix. However, the spatial smoothing-based method can only be applied to that part of the difference co-array that has a contiguous number of elements without any holes, implying that this technique cannot fully utilize the DOFs offered by co-prime arrays.

In [18], multiple frequencies were employed to exploit all of the DOFs of co-prime arrays, thus, increasing the number of resolvable sources. Measurements made at carefully chosen additional frequencies were used to fill in the missing elements in the difference co-array [19]. In doing so, the filled part of the difference co-array is extended, which, in turn, increases the maximum number of sources resolved by high-resolution DOA estimation techniques. However, the increase in DOFs comes with a restriction on the sources' spectra. More specifically, the sources are required to have proportional spectra at the considered frequencies [18,20]. Although this method provides the ability to utilize all of the DOFs of the co-prime array, only a small portion of the additional measurements at frequencies other than the reference frequency are used; the rest are discarded.

In this paper, sparse reconstruction is considered to make use of the full measurement set corresponding to the multi-frequency operation for DOA estimation with co-prime arrays. This enhances the DOFs beyond those offered by a single-frequency operation due to the additional virtual elements generated in the co-array under multi-frequency operation. For sources with proportional spectra, the observations at the different frequencies are cast as a single measurement vector model, which corresponds to a virtual array whose element positions are given by the union set of the difference co-arrays corresponding to the multiple operational frequencies. Sparse reconstruction can then be applied for estimating the directions of signal arrivals. For the case where the sources have nonproportional spectra, the source signal vectors corresponding to the different frequencies have a common support, as the sources maintain their DOA even if their power varies with frequency. The common structure property of the sparse source vectors suggests the application of a group sparse reconstruction. It is noted that sparse recovery was previously applied for DOA estimation with co-prime arrays in [21,22]; however, it was limited to a single-frequency operation and did not consider enhancement of the DOFs of co-prime arrays through multi-frequency operation.

Performance evaluation of the proposed sparsity-based methods is conducted using numerical simulations. We consider three different cases for DOA estimation using sparse reconstruction at multiple frequencies. In the first case, all sources are assumed to have the same bandwidth and all sensors operate at the same multiple frequencies. The second and third cases violate the above assumption with a subset of sensors only operating at multiple frequencies and the sources having nonidentical bandwidth but overlapping spectra.

The remainder of the paper is organized as follows. In Section 2, the multi-frequency signal model for co-prime arrays is presented. In Section 3, the sparse reconstruction-based DOA estimation for multi-frequency co-prime arrays under proportional spectra is discussed. The case of sources with nonproportional spectra is considered in Section 4, and the group sparsity-based reconstruction is presented. The performance of the proposed methods is evaluated in Section 5 through numerical simulations, and Section 6 concludes the paper.

### Notation

Vectors and matrices are denoted by lowercase and uppercase bold characters, respectively. Superscript $(.)^T$ denotes the transpose of a matrix or a vector, whereas their conjugate transpose is denoted by superscript $(.)^H$. The Kronecker product and the Khatri-Rao product [1] are denoted by the symbols $\otimes$ and $\odot$, respectively. $E\{.\}$ denotes the statistical expectation operator, $vec(.)$ denotes the vectorized form of a matrix which is obtained by stacking the columns of the matrix to form a long vector, and bdiag{·} denotes block diagonal matrix.

## 2 Multi-frequency signal model

In its basic configuration, a co-prime array consists of two uniformly spaced linear subarrays. The first subarray has $M$ elements with $Nd_0$ inter-element spacing, and the second one has $N$ elements with $Md_0$ spacing, where $M$ and $N$ are co-prime numbers, and $d_0 = \lambda_0/2$ is the unit spacing with $\lambda_0$ being the wavelength at a reference frequency $\omega_0$ [13]. In this work, we deal with an extended co-prime array configuration, proposed in [15], which has twice the number of elements in one of the subarrays. More specifically, we assume $M$ to be less than $N$ with the first subarray having $2M$ elements, as shown in Figure 1. The elements of the two subarrays are arranged along a single line with the zeroth elements coinciding, resulting in a co-prime array with a total of $(2M + N - 1)$ nonuniformly spaced physical elements. The difference co-array of the extended co-prime array can be expressed as:

$$S_0 = \{\pm(Mnd_0 - Nmd_0)\}, \quad (1)$$

where $0 \le n \le N - 1$, and $0 \le m \le 2M - 1$. The co-array has an aperture of length $2(2M - 1)\,Nd_0$ with contiguous

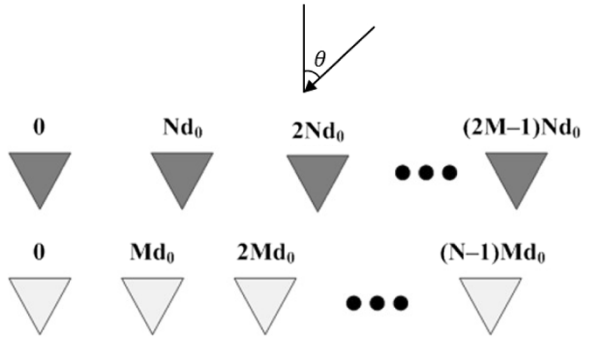


**Figure 1** Extended co-prime array configuration.

elements between $-(MN+M-1)d_0$ and $(MN+M-1)d_0$, as depicted in Figure 2.

Assume that $D$ sources are impinging on the $(2M+N-1)$ – element co-prime array from directions $[\theta_1, \theta_2, \ldots, \theta_D]$, where $\theta$ is the angle relative to broadside. The $(2M+N-1)\times 1$ received data vector is expressed as:

$$\boldsymbol{x}(\omega_0) = \boldsymbol{A}(\omega_0)\boldsymbol{s}(\omega_0) + \boldsymbol{n}(\omega_0), \tag{2}$$

where $\boldsymbol{s}(\omega_0) = [s_1(\omega_0)\ s_2(\omega_0)\ \ldots\ s_D(\omega_0)]^T$ is the source signal vector at $\omega_0$, and $\boldsymbol{n}(\omega_0)$ is the $(2M+N-1)\times 1$ noise vector at $\omega_0$. The $(2M+N-1)\times D$ matrix $\boldsymbol{A}(\omega_0)$ is the array manifold at $\omega_0$, whose columns are the steering vectors corresponding to the sources directions. That is, $\boldsymbol{A} = [\boldsymbol{a}(\theta_1)\ \boldsymbol{a}(\theta_2)\ \ldots\ \boldsymbol{a}(\theta_D)]$ with the steering vector $\boldsymbol{a}(\theta_d)$ corresponding to the direction $\theta_d$ given by:

$$\boldsymbol{a}(\theta_d) = \left[e^{jk_0x_1\sin(\theta_d)}, \ldots, e^{jk_0x_{2M+N-1}\sin(\theta_d)}\right]^T. \tag{3}$$

Here, $k_0 = 2\pi/\lambda_0$ is the wavenumber at the reference frequency $\omega_0$, and $x_i$, $i = 0, 1, \ldots, 2M+N-1$, is the location of the $i$th array element. Assuming that the sources are uncorrelated and the noise is spatially and temporally white with variance $\sigma_n^2$ and uncorrelated from the sources, the autocorrelation matrix of the received data is given by:

$$\begin{aligned}\boldsymbol{R}_{xx}(\omega_0) &= E\left\{\boldsymbol{x}(\omega_0)\boldsymbol{x}(\omega_0)^H\right\}\\ &= \boldsymbol{A}(\omega_0)\boldsymbol{R}_{ss}(\omega_0)\boldsymbol{A}^H(\omega_0) + \sigma_n^2\boldsymbol{I},\end{aligned} \tag{4}$$

where $\boldsymbol{R}_{ss}(\omega_0)$ is the source correlation matrix which is diagonal with the source powers at $\omega_0$, $\sigma_1^2(\omega_0), \sigma_2^2(\omega_0), \ldots, \sigma_D^2(\omega_0)$, populating its main diagonal, and $\boldsymbol{I}$ is a $(2M+N-1)\times(2M+N-1)$ identity matrix. In practice, the autocorrelation matrix is estimated as a sample average of the received signal snapshots.

Following the formulation in [13], the autocorrelation matrix is vectorized as:

$$\boldsymbol{z}(\omega_0) = \mathrm{vec}(\boldsymbol{R}_{xx}(\omega_0)) = \tilde{\boldsymbol{A}}(\omega_0)\boldsymbol{p}(\omega_0) + \sigma_n^2(\omega_0)\tilde{\boldsymbol{i}}, \tag{5}$$

where $\tilde{\boldsymbol{A}}(\omega_0) = \boldsymbol{A}^*(\omega_0) \odot \boldsymbol{A}(\omega_0) = [\boldsymbol{a}^*(\theta_1) \otimes \boldsymbol{a}(\theta_1)\ \ \ldots\ \ \boldsymbol{a}^*(\theta_D) \otimes \boldsymbol{a}(\theta_D)]$, $\boldsymbol{p}(\omega_0)$ is the sources powers vector at $\omega_0$, $\boldsymbol{p}(\omega_0) = \left[\sigma_1^2(\omega_0)\,\sigma_2^2(\omega_0)\ldots\sigma_D^2(\omega_0)\right]^T$, and $\tilde{\boldsymbol{i}}$ is the vectorized form of $\boldsymbol{I}$. The vector $\boldsymbol{z}(\omega_0)$ behaves as the received signal vector at a longer virtual array with sensor positions given by the difference co-array at $\omega_0$ of the physical array. In this model, the sources are replaced by their respective powers and, as such, act as mutually coherent sources, and the noise is deterministic. Traditional subspace-based high-resolution methods, such as MUSIC, can no longer be applied directly to perform DOA estimation. Spatial smoothing can be used to restore the rank of the correlation matrix of $\boldsymbol{z}(\omega_0)$ [23]. However, it can only be applied to the filled part of the difference co-array and the usable DOFs are reduced to approximately one-half of the total number of contiguous co-array elements. Sparsity-based DOA estimation can help extend the usable DOFs to the number of positive lags in the co-array [24].

Consider operating the physical co-prime array at $Q$ different frequencies with the $q$th frequency given by $\omega_q = \alpha_q\omega_0$, where $\alpha_q$ is a constant. Note that it is not required for the reference frequency $\omega_0$ to be one of the $Q$ operational frequencies. If it is included in the operational frequency set, the corresponding $\alpha_q$ assumes a unit value. The received signal at each considered frequency can be extracted by decomposing the array output vector into multiple nonoverlapping narrowband components by using the discrete Fourier transform (DFT) [25,26]. The observation time is assumed to be sufficiently long to resolve the different frequencies.

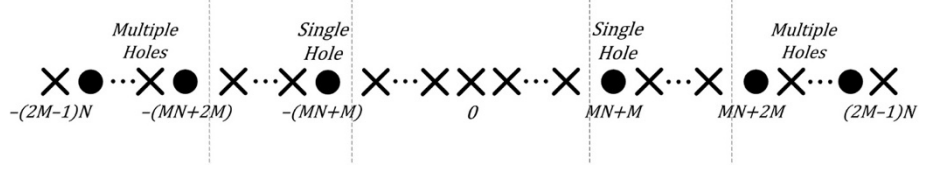


**Figure 2** Difference co-array of the extended co-prime array configuration.

The received signal vector corresponding to the $q$th operational frequency can be expressed as:

$$\boldsymbol{x}(\omega_q) = \boldsymbol{A}(\omega_q)\boldsymbol{s}(\omega_q) + \boldsymbol{n}(\omega_q). \tag{6}$$

Here, $\boldsymbol{s}(\omega_q)$ and $\boldsymbol{n}(\omega_q)$ are the source signal and noise vectors at $\omega_q$, and $\boldsymbol{A}(\omega_q)$ is the array manifold at $\omega_q$ with its $(i, j)$ th element given by:

$$\left[\boldsymbol{A}(\omega_q)\right]_{i,j} = e^{jk_q x_i \sin(\theta_j)},\ k_q = \frac{2\pi\alpha_q}{\lambda_0} = \alpha_q k_0 \tag{7}$$

where $k_q$ is the wave number at $\omega_q$. We observe from (7) that the array manifold at $\omega_q$ is equivalent to the array manifold of a scaled version of the physical co-prime array, with the position of the $i$th sensor in this scaled array given by $\alpha_q x_i$. This, in turn, results in the difference co-array at $\omega_q$ to be a scaled version of the difference co-array of Figure 2 (at the reference frequency $\omega_0$), with $\alpha_q$ being the scaling factor [19]. If $\omega_q$ is higher than the reference frequency, $\omega_0$, the co-array at $\omega_q$ is an expanded version of the one at the reference frequency. On the other hand, for $\omega_q$ lower than $\omega_0$, the equivalent co-array at $\omega_q$ is a contracted version of that in Figure 2. For illustration, consider an extended co-prime array with $M = 3$ and $N = 7$ and the sensor positions given by $[0d_0\ 3d_0\ 6d_0\ 7d_0\ 9d_0\ 12d_0\ 14d_0\ 15d_0\ 18d_0\ 21d_0\ 28d_0\ 35d_0]$. The corresponding difference co-array at $\omega_0$ is shown in Figure 3a. Operating the array at frequency $\omega_1 = 8/7\omega_0$, which is larger than $\omega_0$, results in stretching the difference co-array of Figure 3a, as shown in Figure 3b. On the other hand, if the array is operated at a smaller frequency, say $\omega_1 = 6/7\omega_0$, the difference co-array undergoes contraction as depicted in Figure 3(c).

For multi-frequency DOA estimation, we employ the normalized autocorrelation matrices at each of the $Q$ operational frequencies [20]. The $(i,j)$th element of the normalized autocorrelation matrix $\bar{R}_{xx}(\omega_q)$ is defined as:

$$\begin{aligned}\left[\bar{\boldsymbol{R}}_{xx}(\omega_q)\right]_{i,j} &= \frac{\left[\boldsymbol{R}_{xx}(\omega_q)\right]_{i,j}}{\frac{1}{(2M+N-1)}E\left\{\boldsymbol{x}^H(\omega_q)\boldsymbol{x}(\omega_q)\right\}} \\ &= \frac{E\left\{\left[\boldsymbol{x}(\omega_q)\right]_i\left[\boldsymbol{x}^*(\omega_q)\right]_j\right\}}{\frac{1}{(2M+N-1)}E\left\{\boldsymbol{x}^H(\omega_q)\boldsymbol{x}(\omega_q)\right\}},\end{aligned} \tag{8}$$

where $[\boldsymbol{x}(\omega_q)]_i$ is the $i$th element of the received data vector at frequency $\omega_q$. It can be readily shown that in the normalized autocorrelation matrix $\bar{\boldsymbol{R}}_{xx}(\omega_q)$, the source and noise powers are replaced by their normalized values, which can be expressed as:

$$\bar{\sigma}_k^2(\omega_q) = \frac{\sigma_k^2(\omega_q)}{\sum_{d=1}^{D}\sigma_d^2(\omega_q) + \sigma_n^2(\omega_q)} \tag{9}$$

$$\bar{\sigma}_n^2(\omega_q) = \frac{\sigma_n^2(\omega_q)}{\sum_{d=1}^{D}\sigma_d^2(\omega_q) + \sigma_n^2(\omega_q)} \tag{10}$$

where $\sigma_k^2(\omega_q)$ and $\sigma_n^2(\omega_q)$ denote the respective powers of the $k$th source and the noise at $\omega_q$. Similar to (5), we can express $\bar{\boldsymbol{R}}_{xx}(\omega_q)$ in vectorized form as:

$$\begin{aligned}\bar{\boldsymbol{z}}(\omega_q) &= \mathrm{vec}\left(\bar{\boldsymbol{R}}_{xx}(\omega_q)\right) \\ &= \tilde{\boldsymbol{A}}(\omega_q)\bar{\boldsymbol{p}}(\omega_q) + \bar{\sigma}_n^2(\omega_q)\tilde{\boldsymbol{i}},\end{aligned} \tag{11}$$

where $\bar{\boldsymbol{p}}(\omega_q) = \left[\bar{\sigma}_1^2(\omega_q)\,\bar{\sigma}_2^2(\omega_q)\ldots\bar{\sigma}_D^2(\omega_q)\right]^T$. The measurement vector $\bar{\boldsymbol{z}}(\omega_q)$ emulates observations at the difference co-array corresponding to $\omega_q$.

The measurement vectors $\bar{\boldsymbol{z}}(\omega_q),\ q = 1, 2, \ldots, Q$ can be combined to establish an appropriate multi-frequency linear model that permits DOA estimation within the sparse reconstruction framework. In the sequel, we distinguish two cases of normalized source spectra. In the

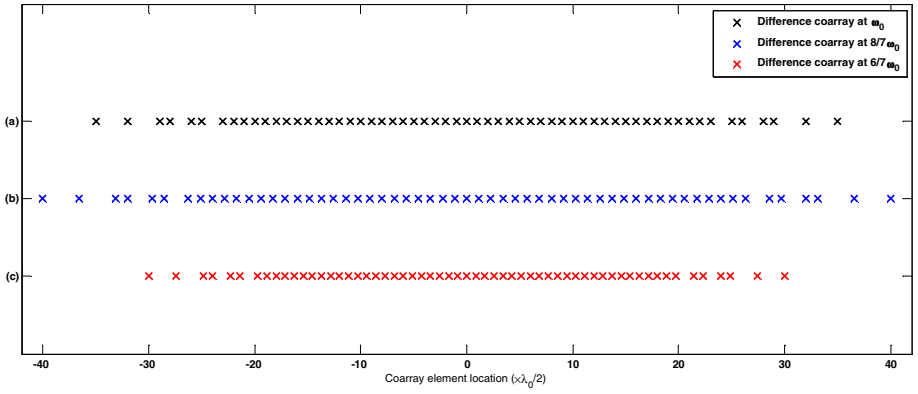


**Figure 3 Difference co-array.** $M = 3$, $N = 7$ **(a)** at $\omega_0$, **(b)** at $\omega_1 = 8/7\omega_0$, and **(c)** at $\omega_2 = 6/7\omega_0$.

first case, we assume the normalized power of each source to be independent of frequency,

$$\bar{\sigma}_k^2(\omega_q) = \sigma_k^2, for all\, k, q, \tag{12}$$

whereas the normalized source powers are allowed to vary with frequency in the second case.

## 3 Sparsity-based DOA estimation under proportional spectra

We discretize the angular region of interest into a finite set of $K \gg D$ grid points, $\{\theta_{g_1}, \theta_{g_2}, ..., \theta_{g_K}\}$, with $\theta_{g_1}$ and $\theta_{g_K}$ being the limits of the search space. The sources are assumed to be located on the grid. Several methods can be used to modify the model in order to deal with off-grid targets [27,28]. Then, (11) can be rewritten as:

$$\bar{\boldsymbol{z}}(\omega_q) = \tilde{\boldsymbol{A}}_g(\omega_q)\bar{\boldsymbol{x}}(\omega_q) + \bar{\sigma}_n^2(\omega_q)\tilde{\boldsymbol{i}}, \tag{13}$$

where the columns of the $(2M+N-1)^2 \times K$ matrix $\tilde{\boldsymbol{A}}_g(\omega_q)$ are the steering vectors at $\omega_q$ corresponding to the defined angles in the grid. The vector $\bar{\boldsymbol{x}}(\omega_q)$ is a $D$-sparse vector whose support corresponds to the source directions with the nonzero values equal to the normalized source powers.

For a high signal-to-noise ratio (SNR), a sufficient condition for (12) to hold is that the sources must have proportional spectra at the employed frequencies [20]. That is:

$$\frac{\sigma_k^2(\omega_q)}{\sigma_l^2(\omega_q)} = \beta_{k,l},\ k, l \in \{1, 2, ..., D\},\ q \in \{1, 2, ..., Q\}. \tag{14}$$

This case is applicable, e.g., when the $D$ sources are BPSK or chirp-like signals. Under proportional source spectra, the source vector $\bar{\boldsymbol{p}}(\omega_q)$ is no longer a function of $\omega_q$, i.e., $\bar{\boldsymbol{p}}(\omega_q) = \bar{\boldsymbol{p}} = \left[\bar{\sigma}_1^2 \bar{\sigma}_2^2 ... \bar{\sigma}_D^2\right]^T$ *for all* $q$, which implies that vector $\bar{\boldsymbol{x}}(\omega_q) = \bar{\boldsymbol{x}}$ for all $q$. As such, the measurement vectors $\bar{\boldsymbol{z}}(\omega_q)$ at the $Q$ operating frequencies can be stacked to form a single $Q(2M+N-1)^2 \times 1$ vector:

$$\bar{\boldsymbol{z}}_g = \tilde{\boldsymbol{B}}_g\bar{\boldsymbol{x}} + \tilde{\boldsymbol{i}}_g, \tag{15}$$

where $\bar{\boldsymbol{z}}_g = \left[\bar{\boldsymbol{z}}(\omega_1)^T \bar{\boldsymbol{z}}(\omega_2)^T ... \bar{\boldsymbol{z}}(\omega_Q)^T\right]^T$, $\tilde{\boldsymbol{i}}_g = [\bar{\sigma}_n^2(\omega_1)\tilde{\boldsymbol{i}}^T\ \bar{\sigma}^{n2}(\omega_2)\tilde{\boldsymbol{i}}^T ... \bar{\sigma}_n^2(\omega_Q)\tilde{\boldsymbol{i}}^T]^T$, and the dictionary $\tilde{\boldsymbol{B}}_g = \left[\tilde{\boldsymbol{A}}_g(\omega_1)^T \tilde{\boldsymbol{A}}_g(\omega_2)^T ... \tilde{\boldsymbol{A}}_g(\omega_Q)^T\right]^T$. The measurement vector is equivalent to that of a virtual array, whose element positions are given by the combined difference co-arrays at the $Q$ frequencies, i.e.,

$$S_g = \{\alpha_1 S_0, \alpha_2 S_0, ..., \alpha_Q S_0\}, \tag{16}$$

where $S_0$ is defined in (1). It is noted that in the case of overlapping points in the $Q$ co-arrays, an averaged value of the multiple measurements that correspond to the same co-array location can be used. This results in a reduction in the dimensionality of $\bar{\boldsymbol{z}}_g$. More specifically, the length of $\bar{\boldsymbol{z}}_g$ becomes equal to the total number of unique lags in the combined difference co-array, which is given by:

$$S_g = \bigcup_{q=1}^{Q} \alpha_q S_0. \tag{17}$$

The dictionary matrix and the noise vector would be changed accordingly.

It should be noted that not all the physical sensors must operate at all $Q$ frequencies. Situations may arise due to cost and hardware restrictions that only a few sensors can accommodate a diverse set of frequencies. The overall difference co-array is still the union of co-arrays at the individual frequencies. However, the difference co-array at each frequency may no longer be a scaled version of the difference co-array at the reference frequency.

Given the model in (15), DOA estimation proceeds in terms of sparse signal reconstruction by solving the following constrained minimization problem:

$$\hat{\boldsymbol{x}} = \arg\min_{\bar{\boldsymbol{x}}} \|\bar{\boldsymbol{x}}\|_1 \text{ subject to } \left\|\bar{\boldsymbol{z}}_g - \tilde{\boldsymbol{B}}_g\bar{\boldsymbol{x}}\right\|_2 < \epsilon \text{ and } \bar{\boldsymbol{x}} \geq 0, \tag{18}$$

where $\epsilon$ is a user-specified bound which depends on the noise variance. The constraint $\bar{\boldsymbol{x}} \geq 0$ forces the search space to be limited to nonnegative values [22]. This is due to the fact that the nonzero elements of $\bar{\boldsymbol{x}}$ correspond to the normalized source powers, which are always positive. This constraint accelerates the convergence of the solution by reducing the search space. Various techniques can be used to solve the constrained minimization problem in (18), examples being lasso, OMP, and CoSaMP [29-31]. In this paper, we use lasso which solves an equivalent problem to (18):

$$\hat{\boldsymbol{x}} = \arg\min_{\boldsymbol{x}} \left[\frac{1}{2}\left\|\bar{\boldsymbol{z}}_g - \tilde{\boldsymbol{B}}_g\bar{\boldsymbol{x}}\right\|_2 + \lambda_t\|\bar{\boldsymbol{x}}\|\right] \text{ subject to } \bar{\boldsymbol{x}} \geq 0 \tag{19}$$

where the $l_2$-norm is the least squares cost function and the $l_1$-norm encourages a sparse solution. The regularization parameter $\lambda_t$ is used to control the weight of the sparsity constraint in the overall cost function. Increasing $\lambda_t$ results in a sparser solution at the cost of an increased least squares error. Several methods have been proposed to

estimate the regularization parameter, such as the discrepancy principle [28,32] and cross validation [29].

The maximum number of resolvable sources using the proposed method depends on the number of unique lags in the combined difference co-array. According to [33], the sparsity-based minimization problem in (19) is guaranteed to have a unique solution under the condition $m \geq 2D$, where $m$ is equal to the number of independent observations or the number of unique lags in the combined difference co-array. As a result, the maximum number of resolvable sources is equal to the number of unique positive lags in the combined co-array. At the reference frequency, the difference co-array extends from $-(2M-1)Nd_0$ to $(2M-1)Nd_0$, and it has a total of $(M-1)(N-1)$ holes, which means that the number of unique lags at each frequency is equal to $(3MN+M-N)$, and the highest number of possible unique positive lags is $(3MN+M-N-1)/2$. Therefore, the maximum number of resolvable sources at each frequency is $(3MN+M-N-1)/2$. Taking into account the overlap between the lags at the different employed frequencies, the maximum number of resolvable sources with the multi-frequency technique is bounded as follows:

$$\frac{(3MN+M-N-1)}{2} < D \leq Q\frac{(3MN+M-N-1)}{2} - (Q-1). \tag{20}$$

The term $(Q-1)$ is subtracted from the upper bound due to the unavoidable overlap between the $Q$ difference co-arrays for the zero lag.

## 4 Sparsity-based DOA estimation under nonproportional spectra

When the source powers vary with frequency, the single measurement vector model of (15) is no longer applicable. However, the $D$ sources have the same directions $[\theta_1, \theta_2, \ldots, \theta_D]$ regardless of their power distribution with frequency. As such, the vectors $\bar{\boldsymbol{x}}(\omega_q)$, $q = 1, 2, \ldots, Q$, in (13) have a common support. That is, if a certain element in, e.g., $\bar{\boldsymbol{x}}(\omega_1)$ has a nonzero value, the corresponding elements in $\bar{\boldsymbol{x}}(\omega_q)$, $q = 2, \ldots Q$, should be also nonzero. The common structure property suggests the application of a group sparse reconstruction. We, therefore, propose a DOA estimation approach based on group sparsity for the nonproportional spectra case.

The received signal vectors $\bar{\boldsymbol{z}}(\omega_q)$ in (13) corresponding to the $Q$ frequencies are stacked to form a long vector:

$$\bar{\boldsymbol{z}}_g = \tilde{\boldsymbol{C}}_g \breve{\boldsymbol{x}} + \tilde{\boldsymbol{i}}_g, \tag{21}$$

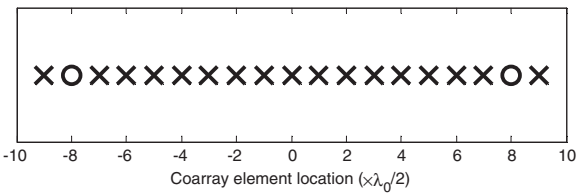


**Figure 4 Difference co-array.** $M = 2$, $N = 3$.

where $\tilde{\boldsymbol{C}}_g = \text{bdiag}\{\tilde{\boldsymbol{A}}_g(\omega_1), \tilde{\boldsymbol{A}}_g(\omega_2), \cdots, \tilde{\boldsymbol{A}}_g(\omega_Q)\}$, and $\breve{\boldsymbol{x}} = \left[\bar{\boldsymbol{x}}(\omega_1)^T \bar{\boldsymbol{x}}(\omega_2)^T \ldots \bar{\boldsymbol{x}}(\omega_Q)^T\right]^T$. The vector $\breve{\boldsymbol{x}}$ is a group sparse vector where each group consists of the source powers corresponding to a specific direction at all operating frequencies. The group sparse solution is obtained by minimizing the following mixed $l_1 - l_2$ norm cost function:

$$min \left\| \bar{\boldsymbol{z}}_g - \tilde{\boldsymbol{C}}_g \breve{\boldsymbol{x}} \right\|_2 + \beta_t \|\breve{\boldsymbol{x}}\|_{2,1} \tag{22}$$

where:

$$\breve{\boldsymbol{x}}_{2,1} = \sum_{i=0}^{K-1} \left[\bar{x}_i(\omega_1), \bar{x}_i(\omega_2), \ldots, \bar{x}_i(\omega_Q)\right]^T{}_2. \tag{23}$$

This means that the variables belonging to the same group are combined using the $l_2$ norm, and the $l_1$ norm is then used across the groups to enforce group sparsity. Different algorithms can be utilized to perform sparse reconstruction with grouped variables. These algorithms include group lasso and block orthogonal matching pursuit (BOMP) [34,35], among many others. In this paper, group lasso is considered to perform DOA estimation in the case of sources with nonproportional spectra. Further, similar to the method discussed in Section 3, a

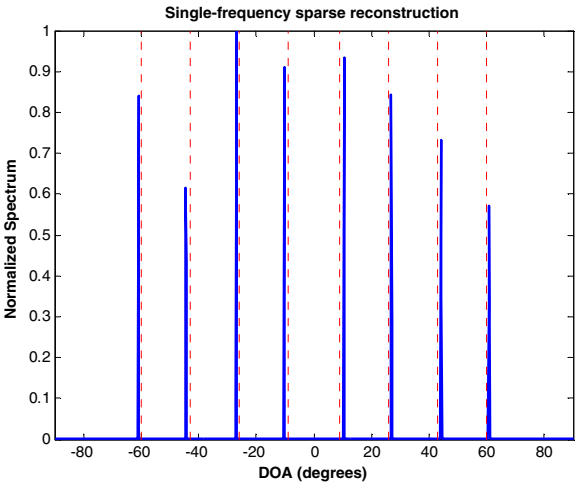


**Figure 5 Single-frequency sparse reconstruction.** $D = 8$ sources.

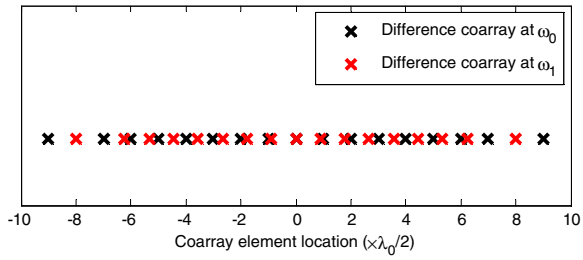


**Figure 6 Dual frequency combined difference co-array.** $\omega_1 = 8/9\omega_0$.

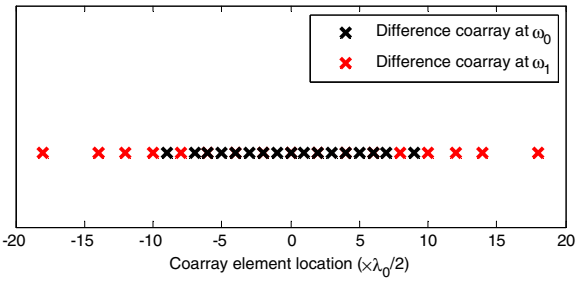


**Figure 8 Dual frequency combined difference co-array.** $\omega_1 = 2\omega_0$.

constraint can be added to force the elements of the solution vector $\tilde{\boldsymbol{x}}$ to be nonnegative.

It is noted that this formulation results in a smaller number of achievable DOFs compared to the case where the sources have proportional spectra. The maximum number of resolvable sources is now limited by the number of observations or unique lags at each frequency [28]. This means that up to $(3MN + M - N - 1)$ sources can be resolved.

## 5 Numerical results

In this section, we present the DOA estimation results for the proposed sparse reconstruction techniques using multi-frequency co-prime arrays and provide performance comparison with the sparsity-based approach for single-frequency co-prime array. We consider both cases of proportional and nonproportional source spectra. For all of the examples in this section, an extended co-prime array configuration with six physical elements is considered with $M$ and $N$ chosen to be 2 and 3, respectively. The six sensor positions are given by $[0, 2d_0, 3d_0, 4d_0, 6d_0, 9d_0]$. The corresponding difference co-array, shown in Figure 4, consists of 17 virtual elements. The co-array aperture extends from $-9d_0$ to $9d_0$ with two holes at $\pm 8d_0$. Further, in all the examples, the choice of the simulation parameters, such as the SNR and the number of snapshots, is typical of radio frequency (RF) applications.

In the first example, sparse signal reconstruction is applied under single frequency operation to perform DOA estimation. Since the difference co-array has eight positive lags, sparse reconstruction can be applied to resolve up to eight sources. A total of eight BPSK sources, uniformly spaced between $-60°$ and $60°$, are considered. The number of snapshots used is 1,000. Spatially and temporally white Gaussian noise is added to the observations, and the SNR is set to 10 dB for all sources. The search space is discretized uniformly between $-90°$ and $90°$ with a $0.2°$ step size, and the regularization parameter $\lambda_t$, is empirically chosen as 0.7 in this example. The normalized spectrum obtained using sparse signal recovery is shown in Figure 5. The dashed vertical lines in the figure indicate the true source directions. A small bias can be noticed in the estimates, and the root mean squared error (RMSE), computed across the angles of arrival, is found to be $1.05°$ in this case.

In the second example, sparse reconstruction is applied under dual-frequency operation. The physical co-prime array is now operated at both frequencies $\omega_0$

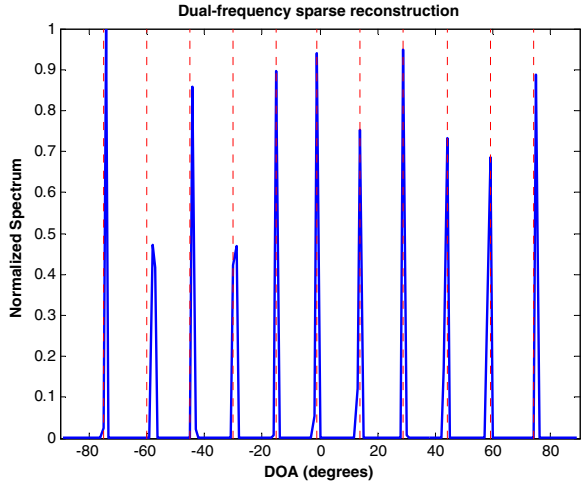


**Figure 7 Dual-frequency sparse reconstruction.** $D = 11$ sources.

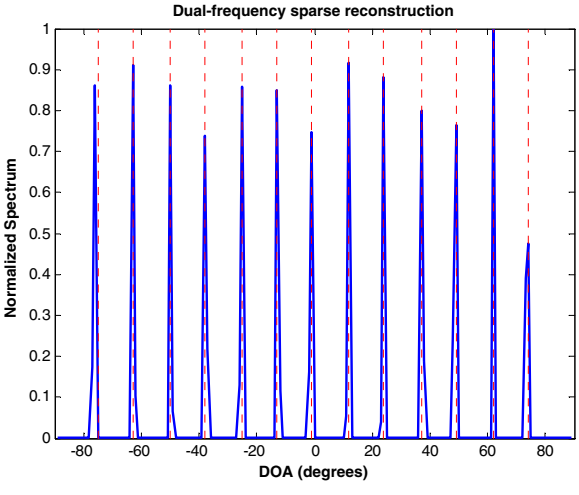


**Figure 9 Dual-frequency sparse reconstruction.** $D = 13$ sources.

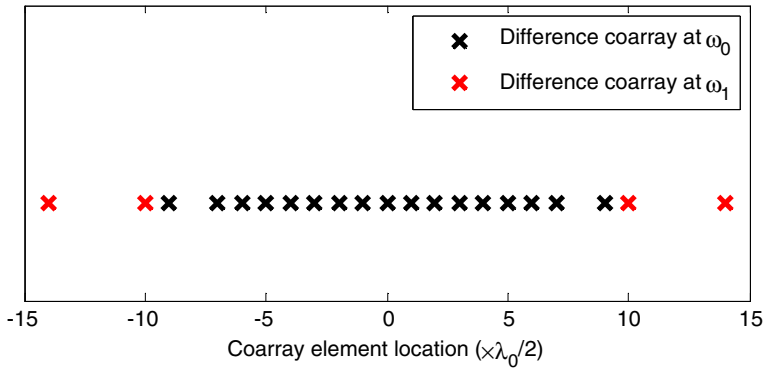


**Figure 10 Dual frequency combined difference co-array.** $\omega_1 = 2\omega_0$.

and $\omega_1 = 8/9\omega_0$. Sources with proportional spectra are assumed, and thus, the single measurement vector formulation of Section 3 can be used. The combined difference co-array is shown in Figure 6. It has a total of 33 unique lags, which makes it capable of resolving up to 16 sources, theoretically. However, this number is not achievable because of the high mutual coherence of the dictionary. Since some of the virtual sensors in the combined co-array are closely separated, leading to highly correlated observations, deterioration in performance is observed if the number of sources is increased beyond 11. We consider 11 BPSK sources with proportional spectra, which are uniformly spaced between −75° and 75°. The SNR is set to 10 dB for the sources at the two frequencies, and the total number of snapshots is equal to 2,000. The regularization parameter $\lambda_t$ is set to 0.25, and the search space is divided into 181 bins of size 1°. Figure 7 shows the normalized spectrum obtained using this method. It is evident that all the sources are correctly resolved. The RMSE in this example is equal to 0.84°. A different choice of the two operational frequencies may reduce the mutual coherence, thereby permitting a larger number of sources to be estimated. For illustration, the second frequency is now set to $\omega_1 = 2\omega_0$. By choosing a frequency which is an integer multiple of $\omega_0$, the combined co-array positions are guaranteed to be integer multiples of $d_0$. As a result, the minimum separation between two consecutive co-array elements is equal to $d_0$. The combined difference co-array is shown in Figure 8. The co-array has 13 unique positive lags, which means that the maximum number of resolvable sources is equal to 13. This is tested by considering 13 uniformly spaced sources between −75° to 75°. The SNR is again set to 10 dB, and the number of snapshots is set to 2,000. The regularization parameter is again set to 0.25, and the search space is divided into 181 angle bins. Figure 9 shows the normalized spectrum using the dual-frequency sparse reconstruction method. It is evident that all the sources are correctly estimated. The RMSE is found to be 0.26° in this case.

In the following example, the entire array is operated at $\omega_0$, but only the elements at $[2d_0\ 4d_0\ 9d_0]$ also operate at the second frequency $\omega_1 = 2\omega_0$. The combined difference co-array is shown in Figure 10, where the difference co-array at $\omega_0$ is shown in black; and the additional lags, obtained by operating the subarray at $\omega_1$, are shown in red. The overall difference co-array has ten positive lags which imply that up to ten sources can be resolved. This is tested by considering ten sources with respective DOAs [−60°, −49°, −29°, −20°, −9°, 3°, 18°, 29°, 47°, 60°]. The number of snapshots is set to 2,000 at each frequency, and the SNR is 10 dB. The regularization parameter is set to 0.7 in this example, and the search space is kept the same. Figure 11 shows the normalized spectrum using the dual-frequency sparse reconstruction method. It can be noticed that all the sources are correctly estimated, and the corresponding RMSE is 0.86°.

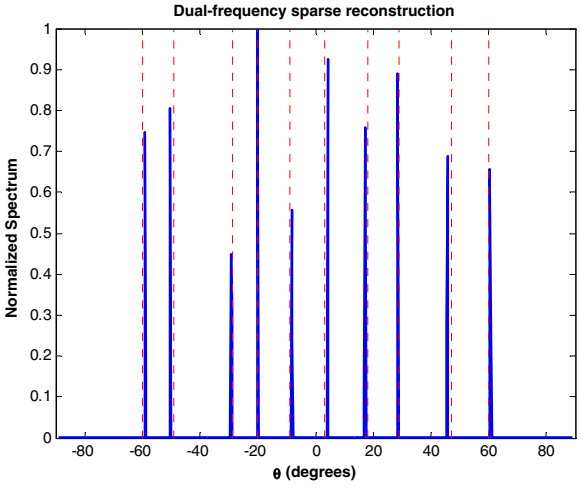


**Figure 11 Dual-frequency sparse reconstruction.** $D = 10$ sources.

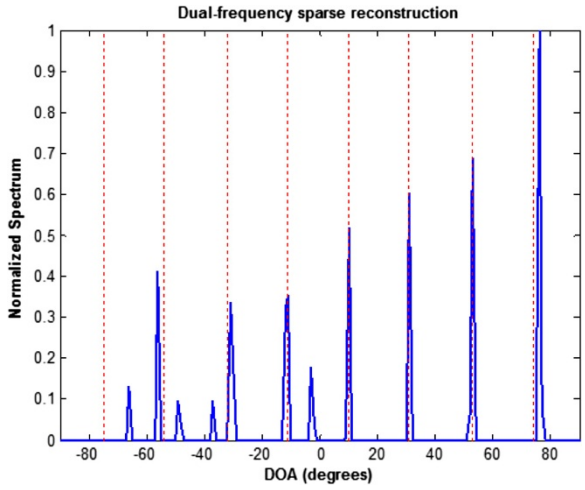


**Figure 12 Dual-frequency sparse reconstruction.** $D = 8$ sources with nonproportional spectra.

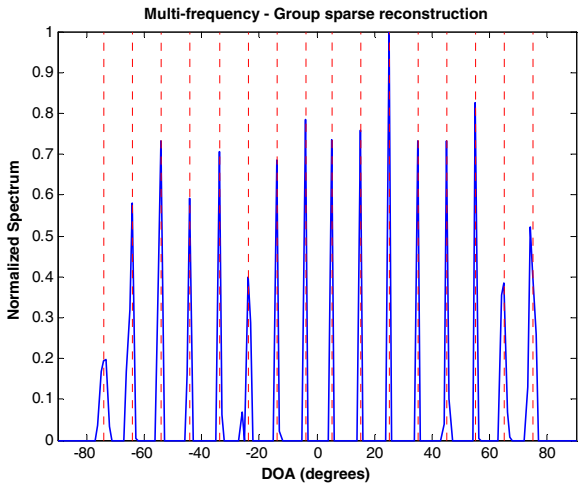


**Figure 14 Multi-frequency group sparse reconstruction.** $D = 16$ sources with nonproportional spectra.

The following example examines the case when sources have nonproportional spectra. In this case, group sparse reconstruction is applied. The two operational frequencies are selected to be $\omega_0$ and $2\omega_0$. Eight sources with nonproportional spectra are considered. The SNR of all the sources at the first frequency is set to 10 dB. At the second frequency, the SNR of each source is a realization of a uniformly distributed random variable between 5 and 15 dB. This ensures that the sources have nonproportional spectra. The noise variance is set to unity at the two frequencies, and a total of 2,000 snapshots are used. Figure 12 shows the normalized spectrum obtained using the formulation in Section 3 which mistakenly assumes proportional source spectra. Consequently, this method is expected to fail as evident in the spectrum of Figure 12. One of the sources is not resolved and several spurious peaks appear in the spectrum. The DOA estimation is next repeated using group sparse reconstruction which was discussed in Section 4. This method does not require the sources to have proportional spectra. The mean of the recovered spectra at the two employed frequencies is computed and shown in Figure 13. It can be seen that group sparse reconstruction is successful in localizing the DOAs of all the sources. The RMSE is found to be 0.6° in this case.

The next example confirms the increase in the number of resolvable sources by using group sparse reconstruction compared to the single-frequency sparse reconstruction. As stated in the first example, the maximum number of resolvable sources using single-frequency sparse reconstruction is equal to the number of unique positive lags in the difference co-array, which is eight in this case. A total of 16 sources with nonproportional spectra is considered in the

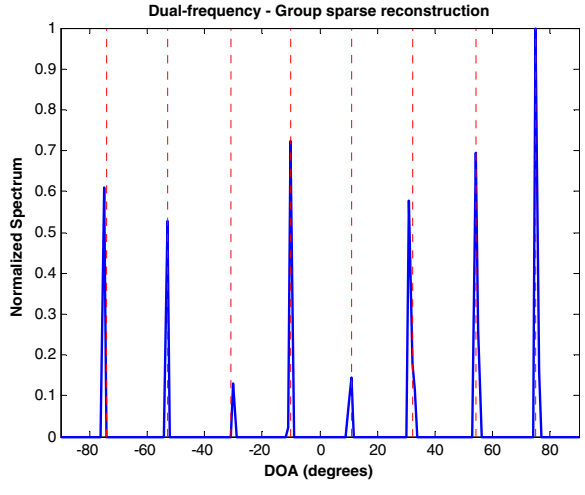


**Figure 13 Dual-frequency group sparse reconstruction.** $D = 8$ sources with nonproportional spectra.

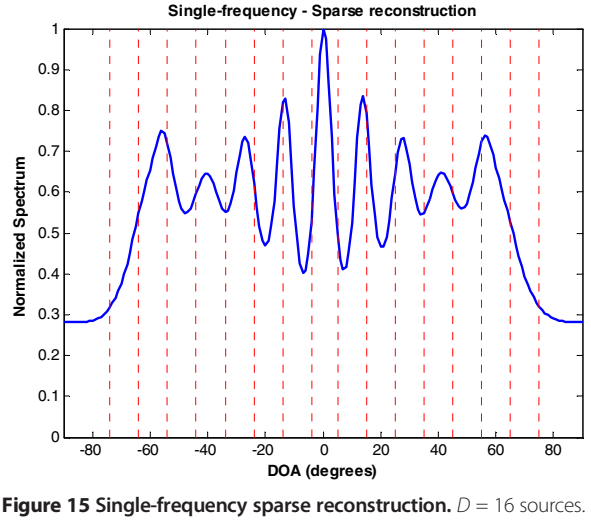


**Figure 15 Single-frequency sparse reconstruction.** $D = 16$ sources.

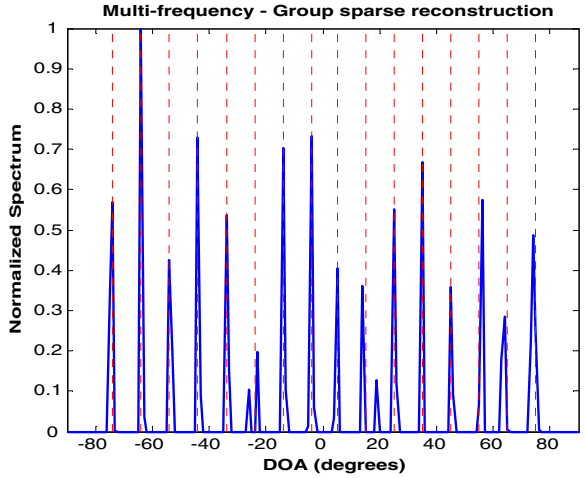


**Figure 16 Multi-frequency group sparse reconstruction.** $D = 16$ sources with nonproportional spectra.

example. The sources are uniformly spaced between −75° and 75°. Twenty uniformly spaced frequencies between $\omega_0$ and $2\omega_0$ are employed. The SNR of each source at each frequency is chosen randomly between −5 and 5 dB, and the number of snapshots at each frequency is set to 1,000. Figure 14 shows the normalized mean spectrum obtained using group sparse reconstruction. It can be seen that all the sources are correctly estimated, and the RMSE is equal to 0.35° in this case. Figure 15 shows the normalized spectrum for the single-frequency sparse reconstruction case. This figure confirms that sparse reconstruction using a single frequency completely fails in estimating the sources. This is due to the fact that single-frequency sparse reconstruction can only resolve up to eight sources which is smaller than the total number of sources in this example.

The final example examines the case where the source signals have overlapping spectra but do not share the same bandwidth. Group sparse reconstruction can still be used to perform DOA estimation. Thirty percent of the source powers at the employed frequencies in the previous example are randomly set to zero. The remaining parameters are kept the same. Figure 16 shows the normalized spectrum using group sparse reconstruction. It is evident that all sources are correctly estimated. Some spurious peaks are present in the spectrum, and an increase in the estimates bias is obtained. The RMSE is found to be 0.61°.

## 6 Conclusions

A sparse reconstruction method has been proposed for DOA estimation using multi-frequency co-prime arrays. The proposed approach offers an enhancement in the degrees of freedom over the single-frequency co-prime array. For sources with proportional spectra, all observations at the employed frequencies are combined to form a received signal vector at a larger virtual array, whose elements are given by the combination of the difference co-arrays at the individual frequencies, thereby increasing the number of resolvable sources. In the case of sources with nonproportional spectra, the common support that is shared by the observations at the employed frequencies is exploited through group sparse reconstruction. Although the offered degrees of freedom are less than those of the multi-frequency approach for proportional spectra, they exceed those offered by single-frequency co-prime array with sparse reconstruction. Numerical examples demonstrated the superior performance of the proposed multi-frequency approach compared to its single-frequency counterpart.

### Abbreviations

CoSaMP: Compressive sampling matched pursuit; DFT: Discrete fourier transform; DOA: Direction of arrival; DOF: Degree of freedom; Lasso: Least absolute shrinkage and selection operator; MHA: Minimum hole array; MRA: Minimum redundancy array; OMP: Orthogonal matching pursuit; RMSE: Root mean squared error; SNR: Signal-to-noise ratio; ULA: Uniform linear array.

### Competing interests

The authors declare that they have no competing interests.

### Acknowledgements

This work was supported by the Office of Naval Research (ONR) under grant N00014-13-1-0061.

Received: 8 July 2014 Accepted: 9 October 2014
Published: 27 November 2014

### References

1. HL Van Trees, *Optimum Array Processing: Part IV of Detection, Estimation, and Modulation Theory* (John Wiley and Sons, New York, 2002)
2. S Chandran, *Advances in Direction-of-Arrival Estimation* (Artech House, Norwood, MA, 2006)
3. TE Tuncer, B Friedlander, *Classical and Modern Direction-of-Arrival Estimation* (Academic Press (Elsevier), Boston, MA, 2009)
4. R Schmidt, Multiple emitter location and signal parameter estimation. IEEE. Trans. Antenn. Propag. **34**(3), 276–280 (1986)
5. R Roy, T Kailath, ESPRIT-Estimation of signal parameters via rotational invariance techniques. IEEE. Trans. Acoust. Speech. Signal. Process. **37**(7), 984–995 (1989)
6. A Moffet, Minimum-redundancy linear arrays. IEEE. Trans. Antenn. Propag. **16**(2), 172–175 (1968)
7. GS Bloom, SW Golomb, Application of numbered undirected graphs. Proc. IEEE **65**(4), 562–570 (1977)
8. C Chambers, TC Tozer, KC Sharman, TS Durrani, Temporal and spatial sampling influence on the estimates of superimposed narrowband signals: when less can mean more. IEEE Trans. Signal Process. **44**(12), 3085–3098 (1996)
9. WK Ma, TH Hsieh, CY Chi, in *Proceedings of the IEEE International Conference on Acoustics, Speech and Signal Processing (ICASSP), 2009*. DOA estimation of quasi-stationary signals via Khatri-Rao subspace (Taipei, Taiwan, 2009), pp. 2165–2168
10. DH Johnson, DE Dudgeon, *Array Signal Processing: Concepts and Techniques* (Prentice Hall, Englewood, NJ, 1993)
11. RT Hoctor, SA Kassam, The unifying role of the coarray in aperture synthesis for coherent and incoherent imaging. Proc. IEEE **78**(4), 735–752 (1990)
12. P Pal, PP Vaidyanathan, Nested arrays: a novel approach to array processing with enhanced degrees of freedom. IEEE Trans. Signal Process. **58**(8), 4167–4181 (2010)
13. PP Vaidyanathan, P Pal, Sparse sensing with co-prime samplers and arrays. IEEE Trans. Signal Process. **59**(2), 573–586 (2011)
14. SU Pillai, Y Bar-Ness, F Haber, A new approach to array geometry for improved spatial spectrum estimation. Proc. IEEE **73**(10), 1522–1524 (1985)

15. P Pal, PP Vaidyanathan, in *Proceedings of the Digital Signal Processing Workshop and IEEE Signal Processing Education Workshop (DSP/SPE)*. Coprime sampling and the MUSIC algorithm (Sedona, AZ, 2011), pp. 289–294
16. YI Abramovich, DA Gray, AY Gorokhov, NK Spencer, Positive-definite Toeplitz completion in DOA estimation for nonuniform linear antenna arrays. I. Fully augmentable arrays. IEEE Trans. Signal Process. **46**(9), 2458–2471 (1998)
17. YI Abramovich, NK Spencer, AY Gorokhov, Positive-definite Toeplitz completion in DOA estimation for nonuniform linear antenna arrays. II. Partially augmentable arrays. IEEE Trans. Signal Process. **47**(6), 1502–1521 (1999)
18. E BouDaher, Y Jia, F Ahmad, M Amin, in *Proceedings of the 22nd European Signal Processing Conference (EUSIPCO), 2014*. Direction-of-arrival estimation using multi-frequency co-prime arrays (Lisbon, Portugal, 2014)
19. F Ahmad, SA Kassam, Performance analysis and array design for wide-band beamformers. J. Electron. Imag. **7**(4), 825–838 (1998)
20. JL Moulton, SA Kassam, in *Proceedings of the 43rd Annual Conference on Information Sciences and Systems*. Resolving more sources with multi-frequency coarrays in high-resolution direction-of-arrival estimation (Baltimore, MD, 2009), pp. 772–777
21. YD Zhang, MG Amin, B Himed, in *Proceedings of the IEEE International Conference on Acoustics, Speech and Signal Processing (ICASSP), 2013*. Sparsity-based DOA estimation using co-prime arrays (Vancouver, Canada, 2013), pp. 3967–3971
22. P Pal, PP Vaidyanathan, in *Proceedings of the 2012 Conference Record of the Forty Six Asilomar Conference on Signals, Systems and Computers (ASILOMAR)*. On application of LASSO for sparse support recovery with imperfect correlation awareness ( Pacific Grove, CA, 2012), pp. 958–962
23. TJ Shan, M Wax, T Kailath, On spatial smoothing for direction-of-arrival estimation of coherent signals. IEEE. Trans. Acous. Speech. Signal. Process. **33**(4), 806–811 (1985)
24. N Hu, Z He, X Xu, M Bao, DOA estimation for sparse array via sparse signal reconstruction. IEEE. Trans. Aerospace. Electron. Syst. **49**(2), 760–773 (2013)
25. H Wang, M Kaveh, Coherent signal-subspace processing for the detection and estimation of angles of arrival of multiple wide-band sources. IEEE. Trans. Acoust. Speech. Signal. Process. **33**(4), 823–831 (1985)
26. Y Yoon, LM Kaplan, JH McClellan, TOPS: New DOA estimator for wideband signals. IEEE Trans. Signal Process. **54**(6), 1977–1989 (2006)
27. Z Tan, A Nehorai, Sparse direction of arrival estimation using co-prime arrays with off-grid targets. IEEE. Signal. Process. Lett. **21**(1), 26–29 (2014)
28. D Malioutov, M Cetin, A Willsky, Sparse signal reconstruction perspective for source localization with sensor arrays. IEEE Trans. Signal Process. **53**(8), 3010–3022 (2005)
29. R Tibshirani, Regression shrinkage and selection via the Lasso. J. Roy. Stat. Soc Ser. B. **58**(1), 267–288 (1996)
30. JA Tropp, AC Gilbert, Signal recovery from random measurements via orthogonal matching pursuit. IEEE. Trans. Informat. Theory. **53**(12), 4655–4666 (2007)
31. D Needella, JA Tropp, CoSaMP: iterative signal recovery from incomplete and inaccurate samples. Appl. Comput. Harmonic. Analysis. **26**(3), 301–321 (2009)
32. VA Morozov, On the solution of functional equations by the method of regularization. Soviet. Math. Doklady. **7**, 414–417 (1966)
33. M Davenport, M Duarte, Y Eldar, G Kutyniok, *Compressed Sensing: Theory and Applications* (Cambridge University Press, Cambridge, UK, 2012), p. 1
34. M Yuan, Y Lin, Model selection and estimation in regression with grouped variables. J. Roy. Stat. Soc. Ser. B. **68**(1), 49–67 (2007)
35. Y Eldar, P Kuppinger, H Bolcskei, Block-sparsity signals: uncertainty relations and efficient recovery. IEEE Trans. Signal Process. **58**(6), 3042–3054 (2010)

doi:10.1186/1687-6180-2014-168
**Cite this article as:** BouDaher *et al.*: Sparse reconstruction for direction-of-arrival estimation using multi-frequency co-prime arrays. *EURASIP Journal on Advances in Signal Processing* 2014 **2014**:168.